Shahangian, N.; Sharifian, L.; Uehara, K.; Noguchi, Y.; Martínez-García, M.; Marti-Aldaravi, P.; Payri, R. (2020). Transient nozzle flow simulations of gasoline direct fuel injectors. Applied Thermal Engineering. 175:1-12. https://doi.org/10.1016/j.applthermaleng.2020.115356

N. Shahangian et al. "Transient nozzle flow simulations of gasoline direct fuel injectors", *Applied Thermal Engineering*, 175, 115356, 2020. DOI: 10.1016/j.applthermaleng.2020.115356

Transient nozzle flow simulations of gasoline direct fuel injectors

Navid Shahangian[a], Leila Sharifian[a], Kazuhiro Uehara[b], Yasushi Noguchi[b], María Martínez[c], Pedro Martí-Aldaraví[c], Raúl Payri[c]

[a]*Advanced Powertrain, Toyota Motor Europe*
[b]*Toyota Motor Corporation*
[c]*CMT-Motores Térmicos, Universitat Politècnica de València*

Abstract

In the field of Internal Combustion Engines (ICE) the usage of Gasoline Direct fuel injectors (GDi) with gasoline, iso-octane, ethanol (or other alternative fuels) has gained relevance in the past years with the goal of reducing fuel consumption and thus emissions. In this type of direct injections, the injector plays a major role in defining the air-fuel mixture quality. Nevertheless, the study of the phenomena inside the nozzle becomes a challenge due to its reduced size, high flow velocities and multiphase flow nature. Computational Fluid Dynamics (CFD) tools allow gaining valuable insight and understanding into such complex flow physics. Therefore, the objective of this work is the development of a predictive methodology for simulating two GDi nozzles. Unsteady Reynolds-Averaged Navier Stokes (URANS) is chosen for modeling the turbulence. The Homogeneous Relaxation Model (HRM) is used to investigate the possible phase change of the fuel through cavitation or flash boiling. Different injection conditions are simulated and results are compared against experimental data of mass flow and momentum rate for validation. CFD is able to accurately predict steady state values, but transients are very dependent on the initial and boundary conditions imposed on the model. A methodology for their definition is proposed and tested, and with it the accuracy in the prediction of the opening transient is improved.

Keywords: GDi, CFD, Nozzle flow, Transient, Predictive model

1. Introduction

Aiming at reducing gasoline engine emissions especially CO_2 and particulate matter (PM) emissions, researches have opted for systems that better control the

fuel injection process into the combustion chamber, such as Gasoline Direct injection (GDi) systems. Nevertheless, the performance of (GDi) engines is still being addressed nowadays [1], especially in transient operation such as vehicle driving cycles. Spark timing and excess of air coefficient have proved to be two main factors affecting the combustion performance, particularly at low loads.

In these GDi systems, the injector plays a major role in engine performance, particularly the nozzle and the injector dynamics. Direct observation of the flow phenomena occurring during the fuel delivery is very challenging due to the reduced size of the orifices (in the order of few hundred microns), the high values of pressure and velocity (up to 30 MPa and 250 m/s) and the short duration of the injection event (few milliseconds or even less). Therefore, computational models are very useful tools to help with the development and optimization of current and new injector nozzles designs. In that direction, it is important to have predictive models that require minimum or no experimental data. This type of models are still under research [2], especially for new GDi systems under engine-like conditions.

Thus, the main objective of this research work is to develop a methodology by means of commercially available Computational Fluid Dynamics (CFD) simulation models for accurate reproduction of hydraulic characteristics of a GDi injector in both steady state and transient operation modes. The CFD software employed is StarCCM+ 12.04. The developed methodology is applied and tested in two different production GDi injectors.

With the aim of create a benchmark for validations, a multi-hole direct fuel injector was made available by the Engine Combustion Network (ECN). The ECN injector, named "Spray G", has been well characterized from the experimental [3, 4, 5] and computational [6, 7] points of view. Rate of injection, spray momentum and near-field spray penetration metrics are measured and used to validate the employed models. Along these years, several experimental studies have been developed in order to study the effects of ambient density or temperature in the vapor generation and plume interaction [8, 9]. Besides, computational studies have been done in parallel in order to model in detail the internal nozzle flow [10] under different conditions, flashing and nonflashing [11, 12, 13, 14]. CFD analysis are going beyond developing Large-Eddy-Simultion (LES) to model the injection process [15, 16, 17]. In the end, the agreement between the simulations and experiments is reasonable for both steady state and transient operations. Hole to hole variations are observed, but they cannot be attributed to needle wobble [11]. Rate of injection oscillations are also noticed [3, 6], which can be attributed to the presence of vapor within the nozzle holes [11]. A similar nozzle has been

studied by Shost et al. [18] with the goal of studying the effects of geometrical parameters, such as length to diameter ratio (L/D), on the spray development. Their experiments and simulations show that both plume direction and spray cone angle are significantly affected by this parameter. Wang et al. [19] used commercial CFD models to understand the effects of deposits on flow pattern and rate of injection of a multi-hole GDi nozzle. Due to the symmetry of the nozzle, they simulated a sector including only one orifice. Their results proved that deposits on the counter-bore restrict the air entrainment and recirculation, and also create additional cavitation inceptions which further reduce the effective outlet area.

During the injection process several complex phenomena occur such as breakup and coalescence which make simulating sprays a challenging task. The traditional and most utilized approach to simulate disperse liquid sprays is the Discrete Droplet Model (DDM) [20, 21, 22]. This approach is thus also known as Eulerian-Lagrangian approach. Several sub-models are required to consider the physical phenomena during injection: atomization, evaporation, collision, coalescence and etc. However, this methodology has proved to provide accurate results when compared to experiments [23]. Although new models developed in recent years which employ a different approach such as Σ-Y Eulerian Atomization Model [24], Eulerian Lagrangian Spray Atomization (ELSA) [25] or Coupled/Decoupled spray simulation [26], a one-way coupling methodology is considered a good approach for spray simulation, which means that data from nozzle flow simulations (e.g. rate of injection and nozzle coefficients) is used as the input for DDM injection sub-model [27].

The currently available models are able to reproduce the experimental trends and hydraulic characteristic parameters of GDi injectors with errors of less than 5% in the discharge coefficient [28] as presented in the 6th meeting of the Engine Combustion Network in Valencia, Spain in September of 2018. However, new researches found different behaviors in the needle opening. The needle lift profile is much slower in the first opening instants, making this behaviour not well captured by the CFD [29]. To the best of the author's knowledge, a fully predictive model and methodology that takes into account this type of behavior has not been developed yet. The present work moves into that direction and focuses on predicting first the rate of injection as well as the spray momentum. The aim is to develop a methodology that provides accurate results to be used as input boundary conditions for spray simulations instead of experimental data [30].

2. Methodology

2.1. Nozzle description

Two different injectors are analyzed, the "Spray G" ECN injector and a Production Injector Unit (PIU). Both of them are solenoid driven with a valve covered orifice (VCO) nozzle. However, they are very different in geometry and performance. For instance, the maximum injection pressure for the Spray G is 23 MPa whilst for the PIU is 28 MPa. Their main characteristics are summarized in Table 1 and represented in Figure 1. The orifice drill angle is measured relative to the nozzle axis, and values of each of the 6 holes (numbered in Figure 2b) of the PIU nozzle are given in Table 2. In order to better visualize the differences, sketches of both nozzles are presented in Figure 2, where the numbering of orifices is also provided. In both cases, the geometry and needle lift profile have been obtained by x-ray and tomography techniques and their corresponding post-processing [4].

Parameter	Spray G	PIU
Bend angle	0°	~ 26°
Number of holes	8	6
Orifice shape	circular	circular
Hole shape	straight	diverging
Nozzle shape	step hole	conical hole
L/D ratio	1.4	2.4
Orifice diameter	165 μm	195 μm
Orifice length	160 − 180 μm	465 μm
Step/Outlet diameter	388 μm	360 μm
Orifice drill angle	0°	variable

Table 1: Main geometrical characteristics of the studied injectors.

Figure 3 compares the needle lift profile of both injectors for similar injection conditions, which are 20 MPa of injection pressure, 363 K of injection temperature, 0.6 MPa of ambient pressure for Spray G and 0.3 MPa for PIU, and 303 K of ambient temperature. The energizing time was 1.5 ms for the PIU and 0.8 ms for Spray G (which were kept constant for the whole study). The hydraulic delay has been removed and the initial time $t = 0$ s is the time needle starts to open. Also, in order to better visualize the differences, lift profiles have been normalized by dividing by their corresponding maximum value, 55 μm for Spray G and about 70 μm for PIU. Needle wobble was also measured, but as suggested by Baldwin

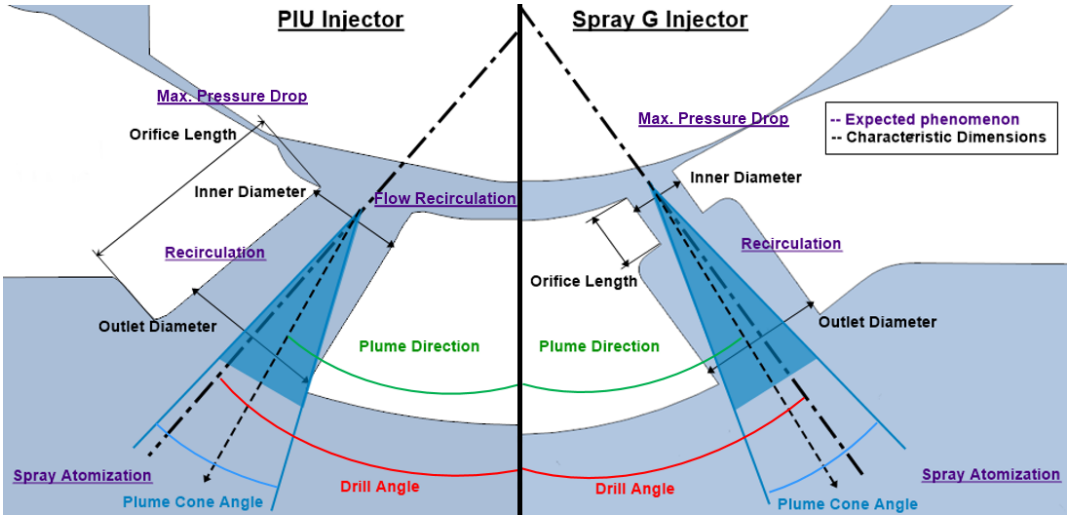

Figure 1: Sketch of the geometrical characteristics of the studied injectors.

Orifice number	Drill angle [°]
1	7.5
2	36
3	53.5
4	44.5
5	53.5
6	36

Table 2: Orifice drill angle for the PIU nozzle relative to nozzle axis.

et al. [11] and Duke et al. [4], and tested for the PIU geometry (see Section 2.4.2), it has negligible effect on rate of injection and spray momentum flux, therefore it is finally not considered in the study. As it is observed in the plot, Spray G injector has faster needle opening and lower oscillations during the steady state operation. Note that the injection duration different in these two cases. Also note that the closing of Spray G is slightly slower than PIU. This may be related to the higher discharge ambient pressure of the presented results.

2.2. Test matrix

Due to different performance and manufacturing characteristics of the two injectors, it was not possible to keep exactly the same test points in both cases.

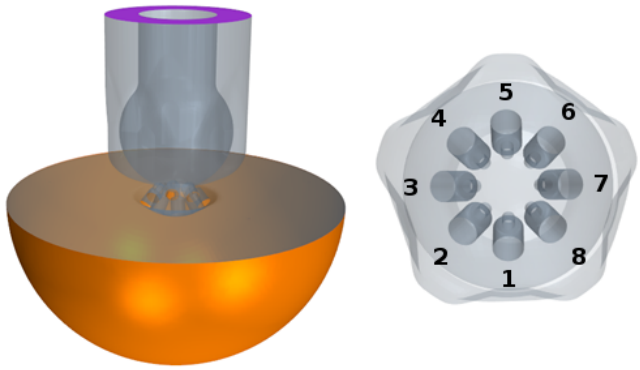

(a) Spray G.

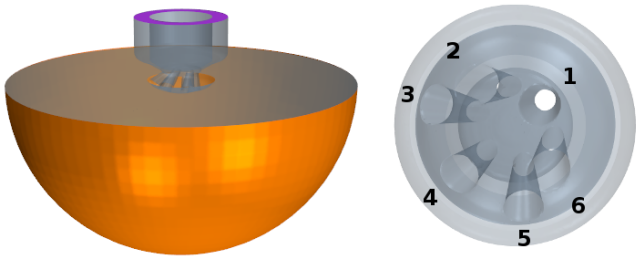

(b) PIU.

Figure 2: Sketch of the nozzle geometry obtained by x-ray beside the computational domain used for the CFD simulation for the two injectors.

Table 3 summarizes the injection conditions used for both experiments and simulations for each of the two geometries. They are relatively wide test matrices, thus simulation results of some of the test points are not performed.

The fuel used for both experiments and simulations is iso-octane (C8H18). It is assumed to be incompressible Newtonian fluid with a density value of 636 kg/m^3, constant dynamic viscosity of $4.806 \cdot 10^{-4} Pa \cdot s$, and also constant specific heat capacity of $2027.59\,J/(K \cdot kg)$. The selection of constant properties can influence the results obtained. However, Giannadakis et al. [31] shown a 3% difference in the discharge coefficient between the use of constant properties and variable properties. Furthermore, in previous studies of this group [32], simulations with constant and temperature-dependent properties were compared by observing similar approximations of mass flow rate and similar spray angles. The effect of the fluid properties could be more visible in the external flow study.

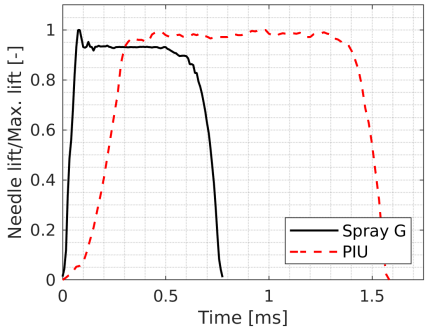

Figure 3: Needle lift profile obtained from x-ray of both injectors for similar injection conditions: p_i = 20 MPa, T_f = 363 K, T_a = 303 K and p_a = 0.6 MPa for Spray G and 0.3 MPa for PIU.

Parameter	Spray G	PIU
Injection pressure (p_i) [MPa]	20	10, 20, 28
Injection temperature (T_f) [K]	363	363
Ambient pressure (p_a) [MPa]	0.6, 0.9, 1.5	0.05, 0.3, 0.6, 1
Ambient temperature (T_a) [K]	303	303
Ambient density (ρ_a) [kg/m^3]	6.67, 10, 16.67	0.56, 3.33, 6.67, 11.12

Table 3: Test matrix of injection conditions for both experiments and simulations.

2.3. Validation experiments

Rate of injection (ROI) was measured using the Bosch method on a commercial EVI (EinspritzVerlaufsIndikator) rate meter. The signal was processed and the cumulative phenomenon corrected. A full description of the experimental setup, including the injector holder with the refrigeration circuit to maintain the fuel temperature constant, can be found in previous work of Payri et al. [3]. This particular experimental technique does not allow measuring below atmospheric pressure as ambient condition, thus, the rate of injection for the cases of 0.05 MPa ambient pressure is not available.

Spray momentum test rig and measurement methodology is also explained in detail in the same work [3]. This technique relies on the whole spray impacting perpendicularly to a force sensor in order to be able to measure the momentum flux. In multi-hole nozzle configuration where sprays can be isolated, momentum of each plume can be measured. However, that is not the case for typical GDi nozzles, where plume-to-plume interactions are strong due to the narrow orifice

drill angles. Payri et al. [3] demonstrated that the integrated results from all holes can be accurately measured. The sensor needs to be placed perpendicular to the injector bend angle, and the measurement must be corrected considering the angle between each of the sprays and the sensor. The distance between the injector tip and the sensor for these measurements is set to 1.5 mm for Spray G and 3 mm for PIU.

Figure 4 shows the experimental rate of injection and momentum flux for the PIU injector obtained with different values of injection and ambient pressures. The maximum differences in the stabilized value is lower than 1.5% for the mass flow rate and about 10% for the momentum flux. In accordance with previous works [3], a decrease in back pressure derives in little increase in mass flow rate.

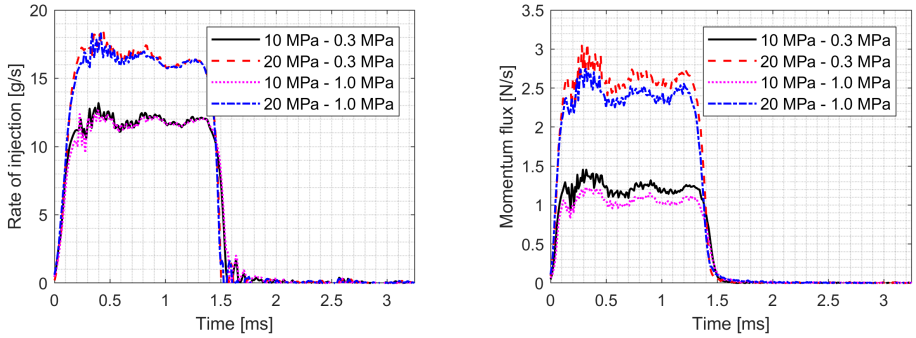

(a) Experimental rate of injection.

(b) Experimental momentum flux.

Figure 4: Example of rate of injection and momentum flux measurements for the PIU injector under different injection and discharge ambient pressure values.

2.4. Model description

2.4.1. Governing equations

An Eulerian framework is employed for simulating the multi-phase fluid inside the nozzle and the near-nozzle spray. The classical conservation equations for mass, momentum and internal energy [33] are solved using a single-fluid approach. Transport equations are solved sequentially with a Segregated Flow Solver and using an Implicit Unsteady Solver loop. An algebraic multigrid (AMG) Linear Solver is used with a relaxation scheme of Gauss-Seidel. The discretization scheme used for computing the convection flux in momentum, energy and species transport equations is first-order backward Euler scheme. The time-steps depends on the Courant-Friedrich-Lewis (CFL) number between $5 \cdot 10^{-7}$ s and

10^{-10} s. The target mean CFL number is selected to 0.5 and the maximum to 5. Three different species are considered in the current work: the liquid fuel, the vapor fuel and the ambient non-condensable gas (N_2). These species are solved first through the species mass fraction transport equation, and then the void fraction is calculated (it is not transported directly). A Volume-of-Fluid interface-capturing method is used to simulate the two-phase (liquid and gas) flow inside the nozzle. A full and detailed description of the employed approach has been previously done by Battistoni et al. [34].

The model for mass exchange between the liquid and vapor phases of the same species is based on the non-equilibrium Homogeneous Relaxation Model (HRM) [35]. It has proved to accurately predict not only cavitation but also flash-boiling. Saha et al. [7] tested the sensibility of the model constants values for a GDi application. The model is employed here following their recommendations.

Regarding the turbulence, a Reynolds-Averaged Navier-Stokes (RANS) approach is selected due to its low computational cost. Therefore, a closure model is required. The Shear-Stress Transport (SST) k-ω [36] is employed. The accuracy of this model is tested later on by comparing the computed nozzle flow coefficients with the experimentally obtained ones.

2.4.2. Computational domain and mesh

Figure 2 shows the computational domain of the simulations. The outlet (orange color in the figure) is a semi-spherical surface with a diameter of 9 mm. This distance is needed in order to avoid the effect of the outlet boundary condition in the solution, and it is accordance with similar nozzle flow studies [6]. The inlet section (purple color in the figure) has been extended upstream for similar reasons.

In all simulations performed in this work the inlet boundary has been modeled using a stagnation inlet condition, applying values of pressure. A specified value stipulated for the temperature has been also defined. Walls (transparent gray in Figure 2) have been modeled with isothermal and non-slip conditions. Reichardt's law is used to compute the near-wall velocity and Kader's law for temperature. The outlet condition has been defined as fixed outlet pressure with zero normal gradient condition for velocity, and as the inlet condition, the temperature has a defined value. Turbulence flow conditions are specified at the inlet (and for the reverse flow at the outlet) boundaries by the turbulent dissipation rate defined by an intensity value of 0.01 and turbulent kinetic energy with a length scale of 0.0001 m. The complete nozzle (holes included) are filled with liquid fuel at constant discharge pressure and injection temperature. The outlet plenum is filled by non-condensable gas at constant discharge pressure and temperature. The exact

values depend on the test point being simulated (see Table 3).

The surface of the needle is moving. Since the computational domain is not split into parts during the simulation, a minimum clearance between the needle and its seat is needed. A value of 2 µm is used for the "closed" position of the needle and the start and end of injection. In order to introduce this movement, the inlet surface is constrained (forced to stay within a plane), the first 100 µm of the needle from the inlet are defined as floating (vertices on the boundary move according to the interpolation of the displacement vector field), and for the rest of the needle the linear displacement is set as the function of time following the obtained needle lift profiles (see an example in Figure 3).

The element type selected is polyhedral because it allows reducing the total cell count to half for similar cell sizes and accuracy of the solution [32]. After a sensitivity analysis of the mesh resolution carried out with the PIU injector and presented in Table 4, the minimum cell size, located inside the orifices and nozzle, was set to 18 µm and the maximum size 60 µm. In both cases, three prism layers with a total thickness of 8.625 µm are attached to the walls obtained a wall y + of 5 as maximum value (some punctual value reaches a wall y+ of 7). The resulting meshes are shown in Figure 5, with a total of 2,296,585 cells for Spray G and 794,444 cells for PIU. This represents only half of the domain because in both cases the geometry is symmetric [11].

Base Size	Min. Cell Size	Cells	ROI	Variation
60 μm	18 μm	0.79 mill.	15.72 g/s	- %
50 μm	15 μm	1.22 mill.	15.81 g/s	0.6 %
40 μm	12 μm	2.60 mill.	15.83 g/s	0.13 %
Experimental			14.88 g/s	

Table 4: Mesh independence results carried out with the PIU injector.

Furthermore, as shown by Duke et al. [4] the wobble does not cause any appreciable change in the flow area into the sac for Spray G. For the PIU nozzle, the effect of needle wobble is tested. Figure 6a adds the measured wobble to the needle lift profile. The y-direction represents a movement from orifice 1 to 4, and the z-direction movement is just perpendicular to it. An additional simulation was carried out with the full geometry of Figure 2b imposing the 3D movement of the needle. The resulting rate of injection compared to a case simulating only the needle lift is given in Figure 6b. The experimental value is also plotted. A zoom in

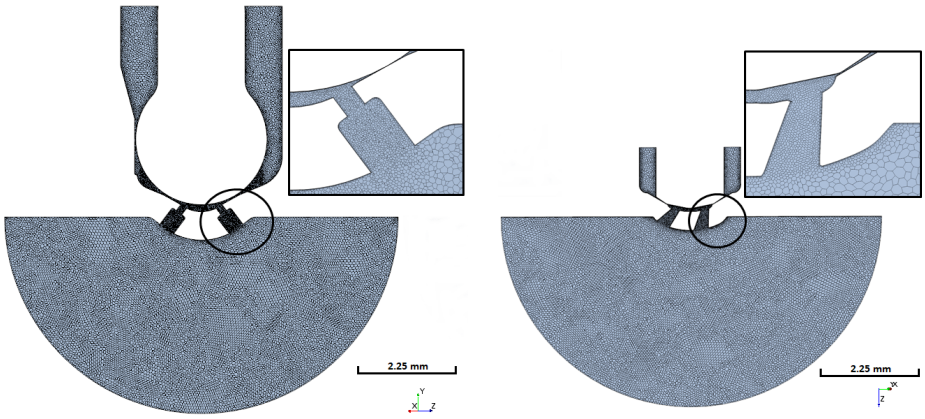

(a) Spray G. (b) PIU.

Figure 5: Sketch of the final mesh in the symmetry plane of the nozzle.

the final part of the needle opening transient is shown in order to better visualize the results. The constant small offset (lower than 2% in the stabilized region) is explained later. Experimentally observed oscillations are not captured by the simulations, not even by imposing the needle lift movements [11, 37]. Even when the y-displacement of the needle is maximum (at about 0.4 ms), the mass flow rate barely changes.

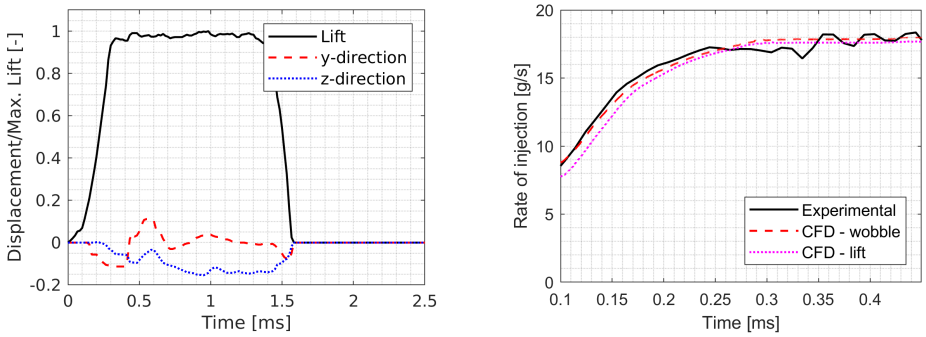

(a) Needle lift and wobble obtained from x-ray analysis.

(b) Rate of injection.

Figure 6: Analysis of the effect of the needle wobble on the PIU injector nozzle flow for the test point of $p_i = 20$ MPa and $p_b = 0.3$ MPa.

In order to better understand the effect of needle wobble and its importance, the averaged steady state hole to hole variation is provided in Table 5, where

simulations results of a case with needle lift and wobble are compared against results of a case with only needle lift (carried out with half of the domain). Except for Hole 1, the difference between the two simulations is low. In fact, the uneven distribution of mass and momentum among the holes is well reproduced by the simulation without imposing the needle wobble. Differences of Hole 1 as well as differences of total rate of injection and momentum flux (which are larger for the momentum than for the mass flow rate) are mainly attributed to the simplification of the geometry (half of the nozzle). The nozzle is not exactly symmetrical by approximately 4 µm, as observed in the x-ray tomography images. As shown in the literature, for steady state operation, the effect of needle wobble on nozzle flow pattern and characteristics can be neglected [11, 38, 39]. It would be significant only for partial needle lift values [40], and perhaps if a time resolved approach of turbulence (i.e Large Eddy Simulations) is employed.

	w/ wobble		w/o wobble		Difference	
	ROI [g/s]	ROM [N/s]	ROI [g/s]	ROM [N/s]	ROI [%]	ROM [%]
Experimental	16.7 ± 0.2	2.5 ± 0.1				
CFD total	17.9	2.95	17.6	2.59	1.50	12.38
Hole 1	3.10	0.602	2.64	0.507	14.8	15.8
Hole 2	3.23	0.636	3.25	0.550	0.67	13.5
Hole 3	2.83	0.539	2.84	0.532	0.18	1.44
Hole 4	2.68	0.512	2.78	0.527	3.87	2.77
Hole 5	2.84	0.563	2.84	0.532	0.11	5.50
Hole 6	3.19	0.557	3.25	0.550	1.96	1.16

Table 5: Steady state values of rate of injection (ROI) and spray rate of momentum (ROM) compared between a complete nozzle domain with needle wobble and half of the domain without needle wobble. The geometry corresponds to the PIU injector, and the injection conditions are p_i = 20 MPa and p_b = 0.3 MPa.

2.5. Simulation strategy

Three different issues arise in these simulations. The first one is related to the computational cost. The computational time step is about 10 ns, and to complete the whole 1.5 ms of injection duration, more than 25000 CPU-h are needed. Furthermore, after the needle reaches its steady state value, no significant change is

observed neither in the rate of injection (see for example Figure 6b) nor the flow pattern and structures. Thus, most of the RANS simulation steady state, a total time of 0.8 ms, is removed in order to save computational cost. An example of the shortened needle lift employed in the reduced calculations is shown in Figure 7a. During the post-process, and for comparison purposes, the steady state of the simulation lengthens the same time as it was removed, as done for the rate of injection shown in Figure 7b.

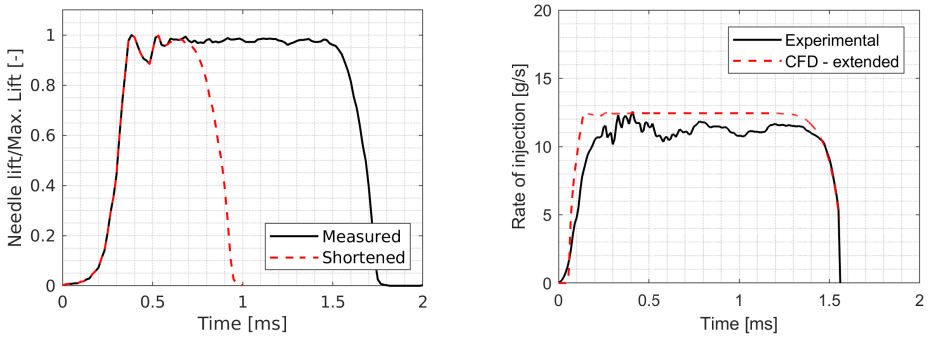

(a) Needle lift. (b) Rate of injection.

Figure 7: Needle lift and rate of injection results of shortening the injection duration strategy for the test point of $p_i = 10$ MPa and $p_b = 0.3$ MPa.

A scalability study was carried out in order to make the most efficient use of the computational resources. The cluster used for this study is built with Intel Xeon E5-2630 v3 CPU, with 8 cores/CPU, 2 CPU/node and 2 GB of RAM/CPU. A steady state case (constant needle lift) with the PIU geometry is selected for this test. The injection pressure is 20 MPa and the discharge ambient pressure is 0.6 MPa. Speedup ($S(n) = T_s(n = 1)/T(n)$) and efficiency ($E(n) = S(n)/n$) are shown in Figure 8 as a function of number of CPU (n). Increasing the number of CPU used for the simulation rapidly decreases the efficiency of the simulation to values slightly above 50%. Nonetheless, the total simulation time is reduced. The speedup process increased going towards using 64 CPU. Thus, 64 CPU are used for all the calculations.

The second issue concerns the selection of inlet boundary condition. As commented in Section 2.4.2, it was set to a constant pressure value. Since the initial conditions of the simulation include a minimum needle lift of 2 µm, the mass flow rate at the orifices outlet rapidly increases to the value corresponding to that needle position. As done in previous works [37], this can be solved by modifying

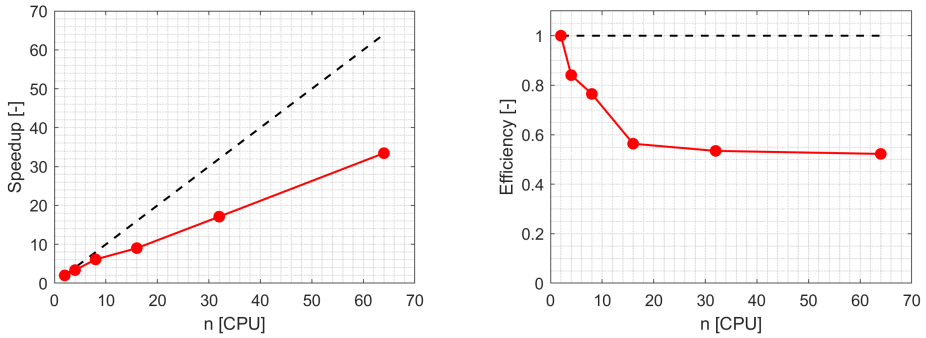

(a) Speedup. (b) Efficiency.

Figure 8: Results of the scalability study performed with the PIU at steady state conditions for the test point of $p_i = 20\,\text{MPa}$ and $p_b = 0.6\,\text{MPa}$.

the inlet pressure time evolution. At the needle opening an expansion wave travels upstream the injector nozzle which temporarily reduces the injection pressure. Duration and intensity of this wave depend not only on the fluid but also on the injector geometry. Thus, for these simulations, it is assumed that the pressure at the inlet rises from the discharge pressure up to the injection pressure during the needle opening. This time is equal to the time it takes for the needle to reach its maximum position. For a fast needle opening, a linear increase provides accurate results [37], however, a parabolic or sinusoidal rise is more similar to one-dimensional simulations of injector performance [41]. An example, for a particular test point, of the pressure signals utilized as inlet boundary condition in the simulation is presented in Figure 9a. Rate of injection results of the three simulations are reported in Figure 9b. The unrealistic mass flow rate at the orifices outlet obtained with a constant inlet pressure is clearly observed in the figure. This effect is reduced when a linear increase of the pressure is used, and almost eliminated with a parabolic rise.

Figure 9b already depicts the third issue. Computational rate of injection is greatly delayed compared to the experimental signal. This delay is attributed to the initial evolution of the needle lift, which can be observed either in Figure 7a or Figure 9a. The needle is lifting very slowly at the beginning (first 0.2 ms), especially at low injection pressures. Nonetheless, this effect is not observed in the mass flow rate experimental measurements where the rising slope of the signal is the same from the start of injection. Furthermore, the uncertainty of the x-ray technique is in the order of $1 - 2\,\mu\text{m}$, which is the value of the needle lift during this time. Therefore, this part of the needle lift could be dismissed, and constant

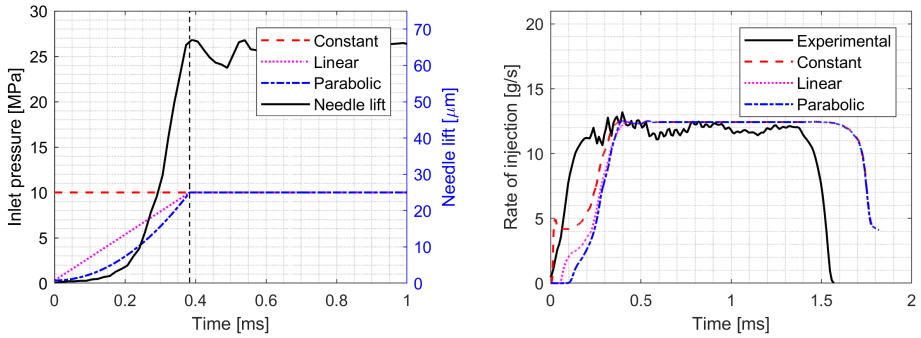

(a) Inlet pressure time evolution.

(b) Rate of injection results.

Figure 9: Effect of changing the inlet pressure time evolution in the simulations considering the effect of pressure drop at the needle opening. Example for the test point corresponding to p_i = 10 MPa, p_b = 0.3 MPa and the PIU geometry.

needle velocity could be assumed for the whole opening transient, but also for the closing transient. This modified needle lift is called “educated needle lift”, and it is shown in Figure 10a. Note that the start of injection is delayed and the injection duration slightly reduced. Results of a simulation carried out with a parabolic initial pressure rise at the inlet and the educated needle lift are shown in Figure 10b. The differences between the experimental and computational profiles are greatly reduced with this methodology. Opening and closing times are now accurately reproduced in the simulations. Only the oscillations of the rate of injection during steady state operation are not captured. Nonetheless, these oscillations are attributed mainly to pressure variations inside the injector [37] and may be also related to unsteady turbulent behavior of the flow.

Even though only one of the test points of the PIU geometry has been used for the explanation of the methodology for the sake of brevity, it is applied also for the Spray G, and of course for all test points.

3. Results

3.1. Validation

Nominal conditions for each geometry are taken as validation test points. These correspond to an injection pressure of 20 MPa for both cases, but a discharge ambient pressure of 0.6 MPa for Spray G and 0.3 MPa for PIU. In the simulations, mass flow rate is calculated at the exit section of the orifices, whilst the spray momentum is obtained as the momentum through a plane perpendicular

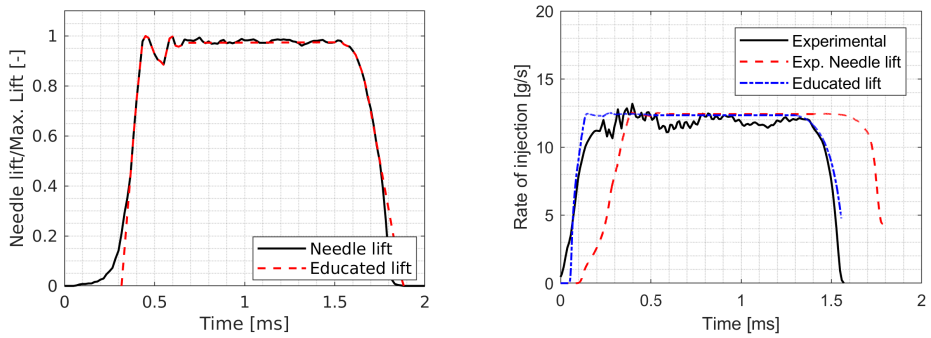

(a) Needle lift from x-ray data.

(b) Rate of injection results.

Figure 10: Effect of changing the needle lift profile to remove the slow initial rising. Example for the test point corresponding to $p_i = 10\,\text{MPa}$, $p_b = 0.3\,\text{MPa}$ and the PIU geometry.

to the injector axis (see Table 1) and located 1.5 mm far from the nozzle tip for Spray G and 3 mm for PIU . This is done in order to reproduce the experiments as explicit as possible.

Figure 11 shows the rate of injection of both geometries compared to experimental results. The accuracy of the proposed model is remarkable in both cases. Rising and closing slopes of the curves are quite similar to the experiments, especially for Spray G whose needle movement is faster (as shown in Figure 3). The steady state value is also well predicted, but it will be better analyzed later by means of nozzle coefficients. As commented before, the experimentally oscillations in the mass flow rate are not reproduced because they could be attributed to variations in pressure upstream the needle [11, 37] and not the needle positioning. They have not been included in the model (see Section 2.5). Those oscillations seem to be of particular significance during the first 300 µs for the Spray G injector, giving a rate of injection lower than the steady state value. The needle overshoot present also in Spray G (see Figure 3) leads to an overshoot in rate of injection, effect of which is reproduced by the simulations. This manifests the sensitivity of these type of injectors to the needle position. Since the needle lift values are generally small compared to other type of injectors, small variations in the lift value may create a strong restriction, limiting the flow capacity of the nozzle.

Experimental and computational rate of momentum are plotted in Figure 12. As before, the experimental results are well predicted by the simulations except for the oscillations during the steady state operation of the injector. The main difference is found at the end of the transient opening where simulations predict an

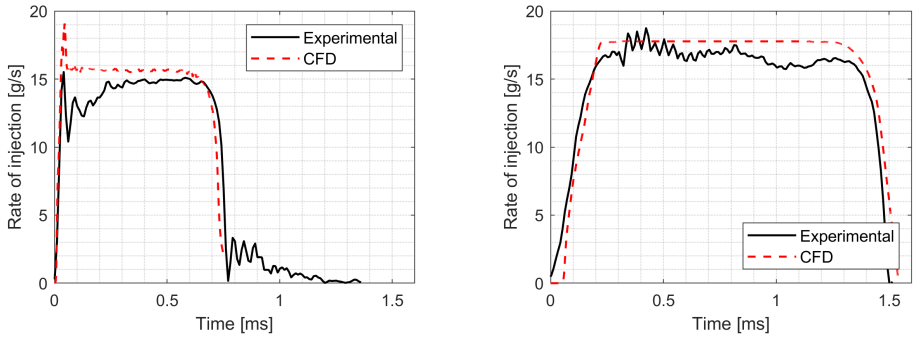

(a) Spray G. (b) PIU.

Figure 11: Computational and experimental rate of injection of both injectors at similar injection conditions: $p_i = 20$ MPa, $T_f = 363$ K, $T_a = 303$ K for both injections, and $p_a = 0.6$ MPa for Spray G and 0.3 MPa for PIU.

overshoot in the signal for both geometries which is not experimentally observed. This effect could be explained by two different reasons:

- Computationally observed overshoot may be due to the initialization inside the nozzle (described at the end of Section 2.4.2) which is probably not exactly the same situation as in the experiments. In fact, exact initial conditions are unknown and may vary from one injection to another. The stagnated fuel inside the orifices is pushed outwards, and temporarily increases the momentum flux through the measuring section.

- The experimental technique includes a plate (for the sensor to measure force of the whole spray) that may alter the transient behavior of the spray. For instance, the hypothesis of the flow being reflected parallel to the surface may be not entirely true for the first droplets arriving to the sensor; those may be reflected in a perpendicular direction.

In order to analyze the steady state operation of the injectors and continue validating the simulations, averaged values of rate of injection and rate of momentum when the needle is fully opened are used to compute the nozzle flow coefficients as defined by Payri et al. [3]: the discharge coefficient (C_d), the velocity coefficient (C_v) and the area coefficient (C_a). These coefficients characterize the flow capacity and hydraulic behavior of the nozzles. Results are summarized in Table 6 together with the total injected quantity for each case. Furthermore, Table 7 represents the existing differences in percentage between experimental and

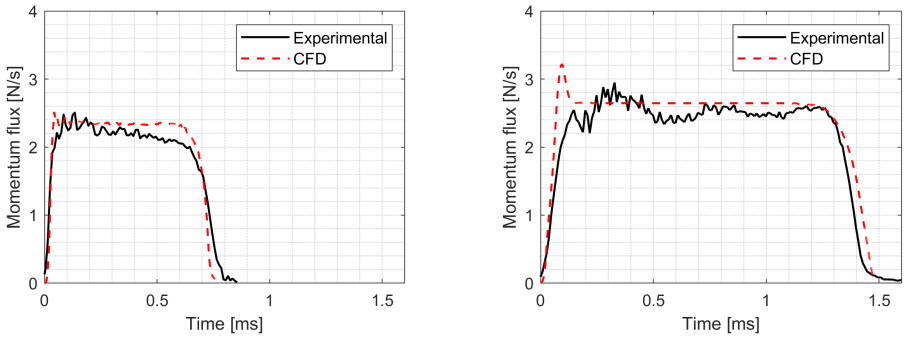

(a) Spray G. (b) PIU.

Figure 12: Computational and experimental rate of momentum of both injectors for similar injection conditions: $p_i = 20\,\text{MPa}$, $T_f = 363\,\text{K}$, $T_a = 303\,\text{K}$ and $p_a = 0.6\,\text{MPa}$ for Spray G and 0.3 MPa for PIU.

computational results. It shows that the injected quantity is systematically overpredicted by 5-6% in the simulations when compared to the experiments. This is mainly due to the oscillations of the rate of injection which are not predicted here. These oscillations reduce the total amount of fuel injected as it can be observed for both geometries in Figure 11.

Consequently, simulations overestimate the nozzle flow coefficients with a maximum difference of 0.04 (which corresponds to ~5%). The fact that the PIU nozzle has slightly higher discharge coefficient is captured by the simulations. However, the trend in velocity coefficient is not reproduced. This can be explained by the overprediction in area coefficient given by the simulations, which is larger for the PIU. Higher effective area leads to a reduction in effective velocity. This means that the flow detachment occurring in the orifice (see Figure 14b) is better captured by the simulations for counter-bore geometries than for diverging orifices. Nonetheless, differences are small and fall within the uncertainty range.

	Inj. quantity [mg]		C_d [-]		C_v [-]		C_a [-]	
Case	Exp.	CFD	Exp.	CFD	Exp.	CFD	Exp.	CFD
Spray G	10.39	11.04	0.55	0.58	0.59	0.61	0.94	0.96
PIU	22.62	23.90	0.59	0.60	0.62	0.60	0.93	0.97

Table 6: Injected quantity and nozzle flow coefficients of both nozzles for nominal conditions of each of them.

Case	Inj. quantity variation	C_d variation	C_v variation	C_a variation
Spray G	6.26 %	5.45 %	3.39 %	2.13 %
PIU	5.66 %	1.69 %	3.23 %	4.30 %

Table 7: Existing differences between experimental and computational injected quantity and nozzle flow coefficients of both nozzles for nominal conditions of each of them.

Flow patterns inside the orifices are represented in Figure 13, where the liquid volume fraction contours are drawn in the symmetry plane of both nozzles (orifices 1 and 5 of Spray G, and 1 and 4 of PIU) together with the velocity vectors. The steady state with the needle fully lifted is selected for the analysis. The liquid fuel does not fill up the orifices, in fact, most of the cross-sectional area of the orifices is occupied by gas. This explains the low discharge coefficients that characterize these type of nozzles. The gas is not vapor fuel but ambient gas (Nitrogen in these cases) which is draged inwards, creating strong recirculation areas inside the orifices. The amount of ambient gas being draged depends not only on the orifice drill angle and their relative position (as shown in Figure 13b), but also on the upstream geometry (which is the difference between the two orifices shown in Figure 13a).

These recirculations areas exert great influence on the spray pattern. Firstly, they clearly deviate the spray from the orifice geometrical axis. The larger the recirculation, the larger the deviation, as clearly shown in Figure 13a. Secondly, being one of the objective of these type of nozzle, they increase the air-fuel mixing. In both geometries, the orifice exit sections do not present a region with only liquid (liquid volume fraction equal to one). The flow velocity is relatively high in these recirculation areas compared to liquid fuel velocity. This effect is clearly seen in Figure 14, where the velocity contours are plotted at two different axial position of all the orifices. In the PIU injector these axial positions are at the entrance and exit of the orifice whereas in the Spray G injector, due to its counterbore shape, the profiles are at the exit of the counterbore and the orifice. The momentum transfer between phases is increased and therefore, as commented before, the air-fuel mixing improves. Emphasize how the zones of maximum recirculation are observed on the outside of the holes. Figure 14 also illustrates the difference in flow between holes, which is more pronounced in the PIU injector than in the Spray G due to the distribution and inclination of the orifices. The velocity observed in the inner profiles is the same as at the exit of the holes due to the similarity in the existing pressure.

3.2. Parametric variation: effect of injection pressure (PIU)

The effect of changing the injection pressure is analyzed in this section. The PIU geometry is selected for the study. Figure 15 represents the rate of injection and momentum flux for the three tested injection pressure values and the same discharge ambient pressure. In these and next plots, the experimental values are represented in black continuous lines regardless of the injection condition to simplify the legend of the graphs. The experimentally observed effects of increasing the injection pressure are very well captured by the simulations:

- As injection pressure increases, the rate of injection and momentum flux also increase, proportional to the pressure drop. The model is able to predict this trend both qualitatively and quantitatively.
- The injection duration is slightly shortened as the injection pressure is increased. This effect is also observed in the simulation results.

Table 8 adds information about the injected quantity and nozzle flow coefficients. Moreover, Table 9 presents the existing differences in percentage between the mentioned results. As commented in Section 3.1, lack of oscillations in the computational curves explains why the injected quantity as well as the discharge coefficient C_d are over-predicted. Nonetheless, the evolution of nozzle flow coefficients when injection pressure changes is well reproduced by the model: velocity coefficient C_v increases and area coefficient C_a decreases as the injection pressure becomes higher. These two effects allow the discharge coefficient to remain almost constant.

	Inj. quantity [mg]		C_d [-]		C_v [-]		C_a [-]	
p_i [MPa]	Exp.	CFD	Exp.	CFD	Exp.	CFD	Exp.	CFD
10	16.86	17.79	0.60	0.60	0.58	0.59	1.02	1.03
20	22.62	23.90	0.59	0.60	0.62	0.60	0.93	0.97
28	25.77	27.59	0.58	0.60	0.63	0.60	0.90	0.95

Table 8: Injected quantity and nozzle flow coefficients of the PIU nozzle for different injection pressure values and a discharge ambient pressure of 0.3 MPa.

p_i [MPa]	Inj. quantity variation	C_d variation	C_v variation	C_a variation
10	5.52 %	0.00 %	1.72 %	0.10 %
20	5.57 %	1.69 %	3.23 %	4.30 %
28	7.06 %	3.45 %	4.76 %	5.56 %

Table 9: Existing differences between experimental and computational injected quantity and nozzle flow coefficients of the PIU nozzle for different injection pressure values and a discharge ambient pressure of 0.3 MPa.

4. Conclusions

Transient simulations of the injection event in two different GDi units have been performed and compared against experimental results under different injection conditions. Three different issues have been addressed and solutions have been proposed:

- Computational cost: in a RANS approach, since the needle lift oscillations are small and have negligible effect on the flow solution, most of the steady state operation is not simulated. This shortens the injection duration and the simulation time. The part which is not simulated is included afterwards during the post-process of the simulation.

- Pressure inlet boundary condition: realistic evolution of upstream value is required as an input to reproduce the experimental shapes of rate of injection and momentum, specially during the transient opening. A parabolic increase from the discharge pressure to the injection pressure during the opening transient is successfully implemented.

- Needle lift profile: x-ray technique provides a lift curve with very low values of lift during the first microseconds of the injection duration. This low lift values restricts the flow and make the simulations results differ from the experimental ones. By removing this small rising of the needle, the accuracy of the simulations improve significantly.

Simulations have shown that GDi injectors are sensitive to the needle position, accurately knowing its value evolution in time allows predictive simulations in terms of rate of injection and momentum. Similarly, the upstream pressure (inlet pressure) plays a major role in the transient behavior of both signals, during the

transients but also for the oscillations in steady state operation. The later was not included in this work.

Low discharge coefficients of GDi nozzles, due either to the counter-bore or the conical shape, propitiate the ambient gas to flow inside the orifices and generate recirculations that enhance the air-fuel mixing. Expected spray cone angles of these type of nozzles are wider than typical straight or converging orifices. A secondary effect of this recirculation is the deviation of the spray axis from the orifice drill angle.

When compared to experiments, the presented simulations report a maximum difference of ~5% in total injected quantity and hydraulic nozzle coefficients for two different nozzles and several injection conditions. The deviation in results could be reduced by bringing the simulation a little closer to the real model by using temperature-dependent fluid properties. Finally, it should be noted that this is the expected error when the described methodology is applied to a different injection condition or nozzle, even though additional tests would be needed to confirm this general applicability.

Acknowledgments

Authors would like to acknowledge Toyota Motor Corporation (TMC) for providing the funds for this project. Authors would like to thank the "Fundación del Centro de Supercomputación de Castilla y León" (FCSCL) and "ACT now HPC Cloud Cluster" for allowing the use of their clusters to perform part of the simulations carried out in this work. Additionally, the Ph.D. student María Martínez has been funded by a grant from the Government of Generalitat Valenciana with reference ACIF/2018/118.

References

[1] Q. Liu, J. Fu, G. Zhu, Q. Li, J. Liu, X. Duan, Q. Guo, Comparative study on thermodynamics, combustion and emissions of turbocharged gasoline direct injection (GDI) engine under NEDC and steady-state conditions, Energy Conversion and Management 169 (May) (2018) 111–123. doi:10.1016/j.enconman.2018.05.047.

[2] B. Befrui, G. Corbinelli, M. D'Onofrio, D. Varble, GDI Multi-Hole Injector Internal Flow and Spray Analysis, SAE Technical Paper 2011-01-1211 (2011). doi:10.4271/2011-01-1211.

[3] R. Payri, J. Gimeno, P. Martí-Aldaraví, D. Vaquerizo, Internal flow characterization on an ECN GDi injector, Atomization and Sprays 26 (9) (2016) 889–919. doi:10.1615/AtomizSpr.2015013930.

[4] D. J. Duke, A. L. Kastengren, K. E. Matusik, A. B. Swantek, C. F. Powell, R. Payri, D. Vaquerizo, L. Itani, G. Bruneaux, R. O. Grover, S. Parrish, L. Markle, D. Schmidt, J. Manin, S. A. Skeen, L. M. Pickett, Internal and near nozzle measurements of Engine Combustion Network "Spray G" gasoline direct injectors, Experimental Thermal and Fluid Science (2017). doi:10.1016/j.expthermflusci.2017.07.015.

[5] L. Zhao, M. Wang, P. Wang, X. Zhu, Q. Qiu, S. Shen, Experimental study on the internal flow field and spray characteristics of hollow nozzle, Applied Thermal Engineering 144 (March) (2018) 757–768. doi:10.1016/j.applthermaleng.2018.06.047.

[6] K. Saha, S. Som, M. Battistoni, Y. Li, E. Pomraning, P. K. Senecal, Numerical Investigation of Two-Phase Flow Evolution of In- and Near-Nozzle Regions of a Gasoline Direct Injection Engine During Needle Transients, SAE International Journal of Engines 9 (2) (2016) 2016–01–0870. doi:10.4271/2016-01-0870.

[7] K. Saha, S. Som, M. Battistoni, Parametric Study of HRM for Gasoline Sprays, ILASS Americas 28th Annual Conference on Liquid Atomization and Spray Systems, Dearborn, MI, May 2016 (May) (2016).

[8] S. E. Parrish, Evaluation of Liquid and Vapor Penetration of Sprays from a Multi-Hole Gasoline Fuel Injector Operating Under Engine-Like Conditions, SAE Technical Paper 2014-04-01 7 (2) (2014) 1017–1033. doi:10.4271/2014-01-1409.

[9] R. Payri, F. J. Salvador, P. Martí-Aldaraví, D. Vaquerizo, ECN Spray G external spray visualization and spray collapse description through penetration and morphology analysis, Applied Thermal Engineering 112 (2017) 304–316. doi:10.1016/j.applthermaleng.2016.10.023.

[10] K. Saha, S. Som, M. Battistoni, Y. Li, S. Quan, P. K. Senecal, Modeling of Internal and Near-nozzle Flow for a GDI Fuel Injector, Proceedings of the ASME 2015 Internal Combustion Engine Division 138 (September) (2015) 1–13. doi:10.1115/ICEF2015-1112.

[11] E. Baldwin, R. Grover, S. Parrish, D. Duke, K. Matusik, C. Powell, A. Kastengren, D. Schmidt, String flash-boiling in gasoline direct injection simulations with transient needle motion, International Journal of Multiphase Flow 87 (2016) 90–101. doi:10.1016/j.ijmultiphaseflow.2016.09.004.

[12] A. Montanaro, L. Allocca, M. Lazzaro, Iso-Octane Spray from a GDI Multi-Hole Injector under Non- and Flash Boiling Conditions (2017). doi:10.4271/2017-01-2319.

[13] Y. Huang, S. Huang, R. Huang, G. Hong, Spray and evaporation characteristics of ethanol and gasoline direct injection in non-evaporating, transition and flash-boiling conditions, Energy Conversion and Management 108 (2016) 68–77. doi:10.1016/j.enconman.2015.10.081.

[14] S. Yang, X. Li, D. L. Hung, M. Arai, M. Xu, In-nozzle flash boiling flow of multi-component fuel and its effect on near-nozzle spray, Fuel 252 (January) (2019) 55–67. doi:10.1016/j.fuel.2019.04.104.

[15] H. Zamani, V. Hosseini, H. Afshin, L. Allocca, M. Baloo, Large Eddy Simulation of GDI Single-hole and Multi-hole Injector Sprays with Comparison of Numerical Break-up Models and Coefficients, Journal of Applied Fluid Mechanics 9 (2) (2016) 1013–1022.

[16] B. Befrui, G. Corbinelli, P. Spiekermann, M. Shost, M. C. Lai, Large Eddy Simulation of GDI Single-Hole Flow and Near-Field Spray, SAE International Journal of Fuels and Lubricants 5 (2) (2012) 620–636. doi:10.4271/2012-01-0392.

[17] Z. Yue, M. Battistoni, S. Som, Spray characterization for engine combustion network Spray G injector using high-fidelity simulation with detailed injector geometry, International Journal of Engine Research 21 (1) (2020) 226–238. doi:10.1177/1468087419872398.

[18] M. Shost, M.-C. Lai, B. Befrui, P. Spiekermann, D. L. Varble, GDi Nozzle Parameter Studies Using LES and Spray Imaging Methods, in: SAE Technical Paper 2014-01-1434, Vol. 1, 2014. doi:10.4271/2014-01-1434.

[19] B. Wang, T. Badawy, P. Hutchins, P. Tu, H. Xu, X. Zhang, Numerical Investigation of the Deposit Effect on GDI Injector Nozzle Flow, Energy Procedia 105 (0) (2017) 1671–1676. doi:10.1016/j.egypro.2017.03.545.

[20] S. C. Kong, P. K. Senecal, R. D. Reitz, Developments in spray modeling in diesel and direct-injection gasoline engines, Oil and Gas Science and Technology 54 (2) (1999) 197–204. doi:10.2516/ogst:1999015.

[21] F. Li; R.D.Reitz;, Spray and Combustion Modeling in Gasoline Direct-Injection Engines, Atomization and Sprays (2000) 10:219–249.

[22] P. K. Senecal, E. Pomraning, Q. Xue, S. Som, S. Banerjee, B. Hu, K. Liu, J. M. Deur, Large Eddy Simulation of Vaporizing Sprays Considering Multi-Injection Averaging and Grid-Convergent Mesh Resolution, Journal of Engineering for Gas Turbines and Power 136 (11) (2014) 111504. doi:10.1115/1.4027449.

[23] M. Battistoni, G. M. Magnotti, C. L. Genzale, M. Arienti, K. E. Matusik, D. J. Duke, J. Giraldo, J. Ilavsky, A. L. Kastengren, C. F. Powell, P. Marti-Aldaravi, Experimental and Computational Investigation of Subcritical Near-Nozzle Spray Structure and Primary Atomization in the Engine Combustion Network Spray D, SAE Technical Paper (2018-01-0277) (2018) 1–15. doi:10.4271/2018-01-0277.

[24] J. M. Desantes, J. M. Garcia-Oliver, J. M. Pastor, A. Pandal, A Comparison of Diesel Sprays CFD Modeling Approaches: DDM versus Σ-Y Eulerian Atomization Model, Atomization and Sprays 26 (7) (2016) 713–737.

[25] K. Saha, P. Srivastava, S. Quan, P. K. Senecal, S. Som, Modeling the Dynamic Coupling of Internal Nozzle Flow and Spray Formation for Gasoline Direct Injection Applications, SAE Technical Paper (2018) 1–13doi:10.4271/2018-01-0314.Abstract.

[26] J. M. Desantes, J. M. Garcia-Oliver, J. M. Pastor, A. Pandal, E. Baldwin, D. P. Schmidt, Coupled decoupled spray simulation comparison of the ECN spray a condition with the Σ-Y Eulerian atomization model, International Journal of Multiphase Flow 80 (2016) 89–99. doi:10.1016/j.ijmultiphaseflow.2015.12.002.

[27] K. Saha, S. Som, M. Battistoni, Investigation of Homogeneous Relaxation Model Parameters and Their Implications for Gasoline Injectors, Atomization and Sprays 27 (4) (2017) 345–365. doi:10.1615/AtomizSpr.2017016338.

[28] R. O. Grover, D. J. Duke, K. E. Matusik, A. L. Kastengren, String Flash-Boiling in Flashing and Non-Flashing Gasoline Direction Injection Simulations with Transient Needle Motion University of Massachusetts Amherst General Motors Research and Development Energy Systems Division , Argonne National Laboratory , Lem, ILASS Americas 28th Annual Conference on Liquid Atomization and Spray Systems (May) (2016).

[29] M. Battistoni, S. Som, C. F. Powell, Highly resolved Eulerian simulations of fuel spray transients in single and multi-hole injectors: Nozzle flow and near-exit dynamics, Fuel 251 (2019) 709–729. doi:10.1016/j.fuel.2019.04.076.

[30] N. Shahangian, L. Sharifian, J. Miyagawa, S. Bergamini, K. Uehara, Y. Noguchi, P. Marti-aldaravi, M. Martinez, R. Payri, Nozzle Flow and Spray Development One-Way Coupling Methodology for a Multi-Hole GDi Injector, SAE Technical Paper Series (2019). doi:10.4271/2019-24-0031.

[31] E. Giannadakis, M. Gavaises, A. Theodorakakos, The influence of variable fuel properties in high-pressure diesel injectors, SAE Technical Paper 2009-01-0832 (2009).

[32] R. Payri, J. Gimeno, P. Marti-aldaravi, M. Martínez, Nozzle Flow Simulation of GDi for Measuring Near-Field Spray Angle and Plume Direction, SAE Technical Paper 2019-01-0280 (2019) 1–11doi:10.4271/2019-01-0280.

[33] J. H. Ferziger, M. Peric, Computational Methods for Fluid Dynamics, 3rd Edition, Springer, Berlin, 2002.

[34] M. Battistoni, D. J. Duke, A. B. Swantek, F. Z. Tilocco, C. F. Powell, S. Som, Effects of noncondensable gas on cavitating nozzles, Atomization and Sprays 25 (6) (2015) 453–483. doi:10.1615/AtomizSpr.2015011076.

[35] D. P. Schmidt, S. Gopalakrishnan, H. Jasak, Multi-dimensional simulation of thermal non-equilibrium channel flow, International Journal of Multiphase Flow (2010). doi:10.1016/j.ijmultiphaseflow.2009.11.012.

[36] F. R. Menter, Zonal Two Equation k-w, Turbulence Models for Aerodynamic Flows, AIAA paper (1993) 1–21doi:10.2514/6.1993-2906.

[37] P. Marti-Aldaravi, K. Saha, J. Gimeno, S. Som, Numerical Simulation of a Direct-Acting Piezoelectric Prototype Injector Nozzle Flow for Partial Needle Lifts, SAE Technical Papers 2017-24-01 (2017). doi:10.4271/2017-24-0101.

[38] Q. Xue, S. Som, M. Battistoni, D. E. Longman, H. Zhao, P. K. Senecal, E. Pomraning, Three-dimensional Simulations of the Transient Internal Flow in a Diesel Injector: Effects of Needle Movement, ILASS Americas (2013).

[39] Q. Xue, S. Som, M. Battistoni, S. Quan, P. K. Senecal, E. Pomraning, D. P. Schmidt, Eulerian CFD Modeling of Coupled Nozzle Flow and Spray with Validation Against X-Ray Radiography Data, SAE International Journal of Engines 7 (2) (2014) 1061–1072. doi:10.4271/2014-01-1425.

[40] M. Battistoni, Q. Xue, S. Som, E. Pomraning, Effect of Off-Axis Needle Motion on Internal Nozzle and Near Exit Flow in a Multi-Hole Diesel Injector, SAE International Journal of Fuels and Lubricants 7 (1) (2014) 1426–2014. doi:10.4271/2014-01-1426.

[41] R. Payri, F. J. Salvador, P. Martí-Aldaraví, J. Martínez-López, Using one-dimensional modeling to analyze the influence of the use of biodiesels on the dynamic behavior of solenoid-operated injectors in common rail systems: Detailed injection system model, Energy Conversion and Management 54 (1) (2012) 90–99. doi:10.1016/j.enconman.2011.10.007.

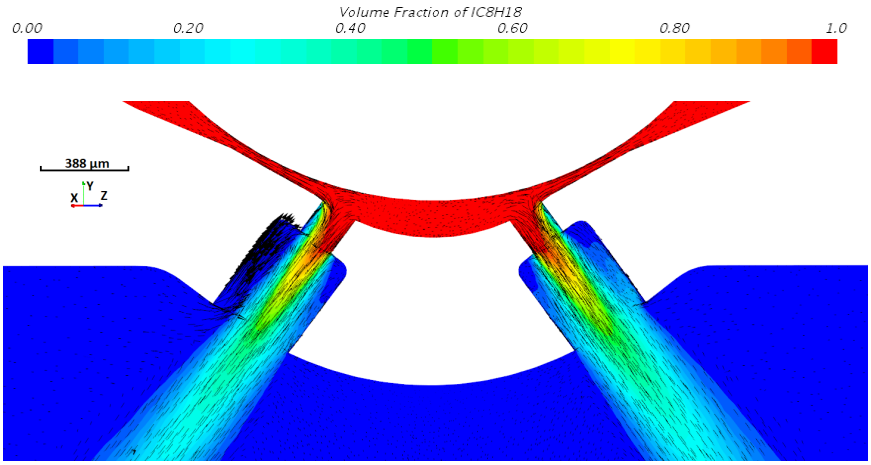

(a) Spray G.

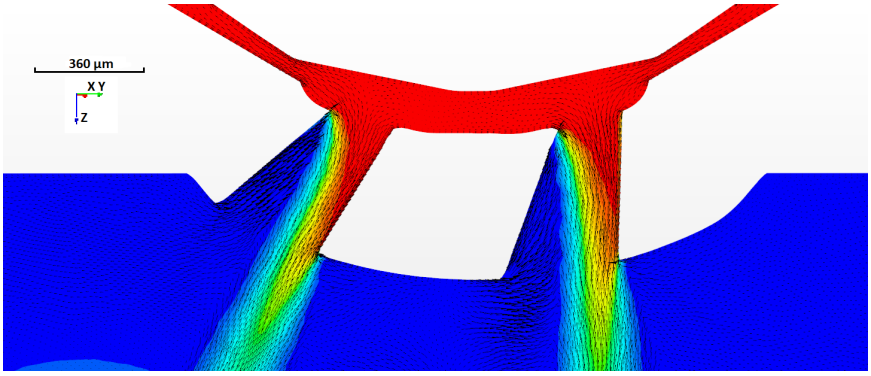

(b) PIU.

Figure 13: Symmetry plane liquid volume fraction contours at steady state condition of both studied geometries. Injection conditions are: $p_i = 20\,\text{MPa}$, $T_f = 363\,\text{K}$, $T_a = 303\,\text{K}$ and $p_a = 0.6\,\text{MPa}$ for Spray G and $0.3\,\text{MPa}$ for PIU.

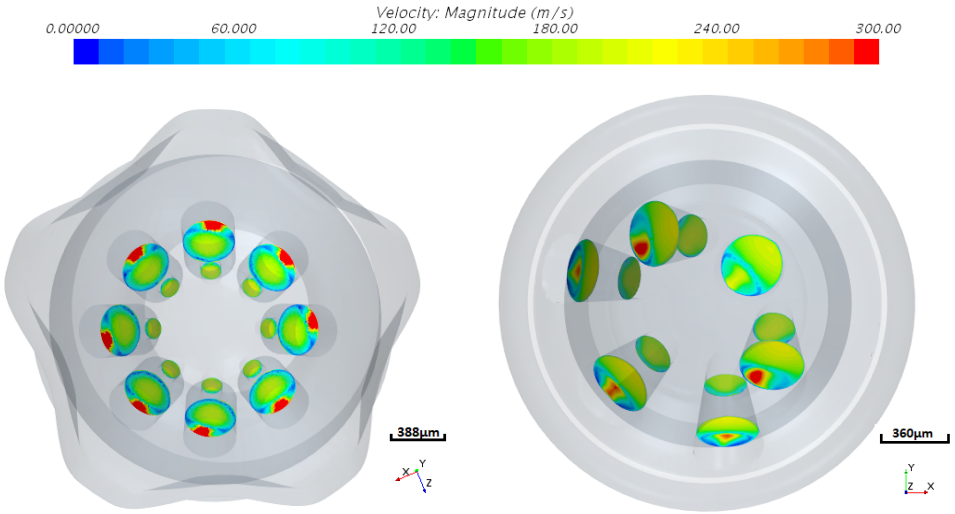

(a) Spray G. (b) PIU.

Figure 14: Orifice cross-sectional velocity contours at steady state conditions of both studied geometries. Injection conditions are: $p_i = 20$ MPa, $T_f = 363$ K, $T_a = 303$ K and $p_a = 0.6$ MPa for Spray G and 0.3 MPa for PIU.

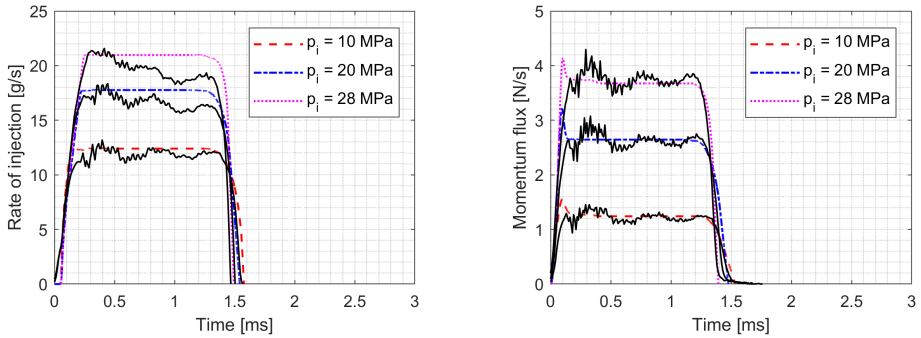

(a) Rate of injection. (b) Momentum flux.

Figure 15: Experimental and computational rate of injection and momentum flux of the PIU nozzle for different injection pressure values and a discharge ambient pressure of 0.3 MPa.